Equilibrium and Kinetic Analysis of Nucleotide Binding to the DEAD-Box RNA Helicase DbpA†

Miguel A. Talavera and Enrique M. De La Cruz*

Yale University, Department of Molecular Biophysics & Biochemistry, 260 Whitney Avenue, New Haven, Connecticut 06520

Received August 12, 2004; Revised Manuscript Received October 11, 2004

ABSTRACT: The *Escherichia coli* DEAD-box protein A (DbpA) is an RNA helicase that utilizes the energy from ATP binding and hydrolysis to facilitate structural rearrangements of rRNA. We have used the fluorescent nucleotide analogues, mantADP and mantATP, to measure the equilibrium binding affinity and kinetic mechanism of nucleotide binding to DbpA in the absence of RNA. Binding generates an enhancement in mant-nucleotide fluorescence and a corresponding reduction in intrinsic DbpA fluorescence, consistent with fluorescence resonance energy transfer (FRET) from DbpA tryptophan(s) to bound nucleotides. Fluorescent modification does not significantly interfere with the affinities and kinetics of nucleotide binding. Different energy transfer efficiencies between DbpA-mantATP and DbpA-mantADP complexes suggest that DbpA adopts nucleotide-dependent conformations. ADP binds ($K_d \sim 50$ μM at 22 °C) 4−7 times more tightly than ATP ($K_d \sim 400$ μM at 22 °C). Both nucleotides bind with relatively temperature-independent association rate constants ($\sim$1−3 μM^{-1} s^{-1}) that are much lower than predicted for a diffusion-limited reaction. Differences in the binding affinities are dictated primarily by the dissociation rate constants. ADP binding occurs with a positive change in the heat capacity, presumably reflecting a nucleotide-induced conformational rearrangement of DbpA. At low temperatures (<22 °C), the binding free energies are dominated by favorable enthalpic and unfavorable entropic contributions. At physiological temperatures (>22 °C), ADP binding occurs with positive entropy changes. We favor a mechanism in which ADP binding increases the conformational flexibility and dynamics of DbpA.

Members of the DEAD-box[1] family of proteins are enzymes that couple unwinding of double-stranded RNA with ATP hydrolysis and participate in all levels of RNA metabolism (*1*). Genomic sequencing efforts have identified DEAD-box proteins in viruses, bacteria, and eukaryotes including yeast and humans. The ability to unwind stretches of duplex RNA (*2*), disrupt RNA−protein interactions (*3*), and assist in the correct *in vitro* folding of RNA (*4*) enables DEAD-box proteins to participate in a diverse array of cellular processes including splicing, ribosome biogenesis, RNA degradation, RNA interference, and translation (*5*).

In contrast to the well-characterized DNA helicases, detailed mechanistic studies of DEAD-box RNA helicases have proven difficult due to poor nucleic acid substrate specificity and low activities of purified proteins (*5*, *6*). In addition, most DEAD-box proteins are likely to function as part of macromolecular assemblages and require additional accessory components for optimal activity (*5*, *6*).

The ATPase activity of *Escherichia coli* DEAD-box protein A (DbpA) is specifically activated by nanomolar concentrations of 23S ribosomal RNA subfragments that include hairpin 92 (*7*), an essential component of the peptidyl-transferase center (PTC). High RNA substrate specificity in the absence of accessory proteins makes DbpA an excellent model system to study the molecular mechanism of DEAD-box protein activity.

Detailed mechanistic studies of nucleotide binding, hydrolysis, and product release are necessary for understanding the mechanism of energy transduction and defining how ATP binding and hydrolysis are coupled to the conformation of DbpA (*8*) and the rearrangements of RNA structure. Although the RNA sequence requirements for DbpA activity have been characterized in detail (*2*, *7*, *9*, *10*), the mechanisms of nucleotide binding and hydrolysis are not well defined. In this study, we have used fluorescently modified mant-nucleotides to characterized the kinetics and equilibrium binding of DbpA with adenine nucleotides. Our results provide the mechanism of nucleotide binding to DbpA and establish a kinetic and thermodynamic framework for defining the mechanism of PTC−RNA activation of DbpA.

EXPERIMENTAL PROCEDURES

Reagents. All chemicals were of the highest purity commercially available. ATP (99+% purity as assayed by

† This work was supported by a Hellman Family Fellowship (to E.M.D.L.C.), and by grants from the National Science Foundation (to E.M.D.L.C.) and the American Heart Association (to E.M.D.L.C.). M.A.T. was supported by an NIH NRSA predoctoral fellowship (GM6460-02).

* To whom correspondence should be addressed. Telephone: (203) 432-5424; fax: (203) 432-1296; e-mail: enrique.delacruz@yale.edu.

[1] Abbreviations: ϵ_x, molar extinction coefficient at wavelength x in units of nanometers; λ_{em}, emission wavelength; λ_{ex}, excitation wavelength; Abs, absorbance; ADP, adenosine 5′-diphosphate; ATP, adenosine 5′-triphosphate; DbpA, DEAD-box protein A; DTT, dithiothreitol; f_{cor}, correction factor; FI, fluorescence intensity; FRET, fluorescence resonance energy transfer; GuHCL, guanidium chloride; HEPES, 4-(2-hydroxyethil)-1-piperazineethanesulfonic acid; HPLC, high performance liquid chromatography; K_d, equilibrium dissociation constant; k_{obs}, observed pseudo-first-order rate constant; mantADP or mD, 2′- (or -3′)-*O*-(*N*-methylanthraniloyl) adenosine 5′-diphosphate; mantATP or mT, 2′- (or -3′)-*O*-(*N*-methylanthraniloyl) adenosine 5′-triphosphate; P_i, inorganic phosphate; PTC, peptidyl transferase center; rRNA, ribosomal RNA; U, unlabeled nucleotide.

10.1021/bi048253i CCC: $30.25
Published on Web 12/17/2004

HPLC, data not shown) was purchased from Roche Molecular Biochemicals (Indianapolis, IN) and ADP (Sigma A-5285, 99+% purity as assayed by HPLC, data not shown) was purchased from Sigma (St. Louis, MO). ATP and ADP concentrations were determined by absorbance at 259 nm using ϵ_{259} of 15 400 M^{-1} cm^{-1}. *N*-Methylanthraniloyl-nucleotides (mantADP and mantATP, mixed 2′ and 3′ isomers) were synthesized as described (*11*) or purchased from Molecular Probes (Eugene, OR). Mant-nucleotide concentrations were determined using ϵ_{255} of 23 300 M^{-1} cm^{-1}. A molar equivalent of $MgCl_2$ was added to nucleotide solutions immediately before use. All experimental measurements were made in buffer A (100 mM NaCl, 5 mM $MgCl_2$, 1 mM DTT, 20 mM HEPES, pH adjusted to 7.5 at the experimental temperature).

Protein Purification. DbpA was purified as described (*2*). Briefly, DbpA was overexpressed in *E. coli* strain BL21-(DE3) pLys-S and purified by ion exchange (DEAE-Sepharose and SP-Sepharose, 10 × 2.5 cm, Pharmacia) and size exclusion (Superdex 75-HiLoad 16/60, 1.6 × 60 cm, Pharmacia) chromatography. Yields varied between from ~20 to 35 mg/L culture. The DbpA concentration was determined by absorption at 280 nm in buffer A using an ϵ_{280} of 25 200 $M^{-1}cm^{-1}$ for DbpA, which was determined by comparison with the absorbance (Abs) of denatured DbpA in 6 M GuHCl using the following relationship (*12*):

$$\epsilon_{\text{native}} = \frac{(\text{Abs}_{\text{native}})(\epsilon_{\text{denatured}})}{(\text{Abs}_{\text{denatured}})} \quad (1)$$

The ϵ_{280} of DbpA in 6 M GuHCl ($\epsilon_{\text{denatured}}$) was calculated from the ϵ of the predicted amino acid sequence determined under similar conditions. Experiments were performed within 5 days of purification.

Steady-State ATPase Activity. The steady-state ATPase activity of DbpA was measured at 37 °C in buffer A supplemented with 2 mM MgATP using the malachite-green P_i detection assay (*13*). The PTC−RNA-activated ATPase activity was measured using a 153-nucleotide fragment of the *E. coli* 23S rRNA spanning nucleotides 2454 through 2606 of the rRNA gene (*10*).

Equilibrium Binding. Steady-state fluorescence measurements were measured in buffer A at 22 (± 1) °C with a Photon Technologies Intl. (South Brunswick, NJ) Quantamaster fluorescence spectrometer using a 0.3 × 0.3 cm Suprasil quartz cuvette (Hellma Ultra-Micro Cell, GmbH & Co KG, Müllheim, Germany). When monitoring tryptophan fluorescence or energy transfer from tryptophan residues to the mant fluorophore, an excitation wavelength of 297 nm was used to minimize inner-filter effects arising from absorbance by the nucleotide. To assess the energy transfer efficiency, mant-nucleotide fluorescence was also monitored with excitation at 340 nm.

Observed fluorescence intensities were corrected ($FI_{cor} = FI_{obs}f_{cor}$) for inner-filter effects assuming that the light sampled emanates from a point in the center of the cell (*14*). The correction factor (f_{cor}) was calculated using eq 2:

$$f_{\text{cor}} = 10^{((\Delta A_{\text{ex}} + \Delta A_{\text{em}})/2)} \quad (2)$$

where ΔA_{ex} and ΔA_{em} are the additional absorbance at the excitation (297 nm) and emission (340 nm) wavelengths. Data used were limited to conditions where $A < 0.3$ (*15*).

The nucleotide concentration dependence of the corrected steady-state fluorescence intensities was fitted to a rectangular hyperbola in the form of eq 3, which assumes DbpA possesses a single nucleotide-binding site (defined by the Walker A and Walker B motifs, ref *16*):

$$\text{FI} = \text{FI}_o + \frac{(\text{FI}_\infty - \text{FI}_o)[\text{mD}]_F}{K_d + [\text{mD}]_F} \quad (3)$$

where FI is the background and inner-filter corrected fluorescence intensity, FI_o is the fluorescence of DbpA alone, FI_∞ is the fluorescence of DbpA with bound mantADP, $[mD]_F$ is the free mantADP concentration ($[mD]_T \gg [DbpA]$, therefore $[mD]_T \sim [mD]_F$), and K_d is the dissociation equilibrium constant for nucleotide binding to DbpA. The K_d and the amplitude ($FI_\infty - FI_o$) were unrestrained when fitting.

The equilibrium binding affinities of unlabeled nucleotides were measured by competition with mantADP. Because of the weak affinity of the protein for mantADP and the high inner filter effects at the excitation wavelength, an equilibrated sample of 2 μM DbpA and 50 μM mantADP (~50% saturation) was titrated with increasing amounts of unlabeled nucleotide. The [ADP] dependence of the reduction in the corrected fluorescence (FI) was fitted to eq 4:

$$\text{FI} = \text{FI}_o + \frac{(\text{FI}_\infty - \text{FI}_o)[\text{DbpA} - \text{mD}]}{[\text{mD}]_T} \quad (4)$$

where FI is the corrected fluorescence intensity at 430 nm (λ_{ex} = 297 nm), FI_o is the fluorescence measured in the absence of competing unlabeled nucleotide, FI_∞ is the fluorescence in the presence of saturating unlabeled nucleotide, $[mD]_T$ is the total mantADP concentration, and [DbpA−mD] is the concentration of DbpA with bound mantADP. There are two unknown variables in eq 4: FI_∞ and [DbpA−mD]. Because under our conditions DbpA is not completely saturated, a fraction exists free in solution and assumptions that simplify analysis of competition binding data to hyperbolic or quadratic forms (*17*) cannot be applied. Therefore, the concentration of DbpA−mD was determined by solving the cubic equation (Appendix I) defining the reversible, competitive binding of two ligands for a single site, obtained by accounting for all partial equilibria present in the system and noting that the mass conservation of total protein ($[P]_T$) is described by the sum of free and bound species ($[P]_T = [P]_F + [PmD] + [PU]$). The analysis requires prior knowledge of the affinity of one ligand (mantADP or unlabeled nucleotide). To solve for [DbpA−mD], the regression equations were programmed into Igor (version 5.0, WaveMetrics, Inc., Lake Oswego, OR) and the data were fitted using the cubic solution when the affinity of unlabeled is weaker than labeled ($K_U > K_{mD}$; eq A1.16) or when the unlabeled binds more tightly ($K_U < K_{mD}$; eq A1.17) and constraining the values of FI_o and the dissociation constant of the DbpA−mantADP complex (K_{mD}) measured independently (Figure 2, Table 1). The value of FI_∞ and the affinity for unlabeled nucleotide (K_U) were floated during the fitting process. The value of FI_∞ is obtained from the best fit to eq 4.

Table 1: Rate and Equilibrium Constants for Nucleotide Binding to DbpA[a]

nucleotide	temp (°C)	k_+ ($\mu M^{-1} s^{-1}$)	k_- (s^{-1})	K_d^{kin} (μM)[b]	K_d^{ttn} (μM)
mantADP	22	3.4 (± 0.2)	180 (± 4)[c] 176 (± 2)[d]	52 (± 3)	54 (± 14)[d] 70(± 14)[e]
mantATP	22		>360		
ADP	22				47 (± 6)[e] 70 (± 25)[f]
ATP	22				~400[f]
mantADP	4	2.4 (± 0.1)	62 (± 4)[c] 58 (± 2)[d]	26 (± 2)	
mantATP	4	0.77 (± 0.02)	65 (± 2)[c] 70 (± 4)[d]	84 (± 2) 91 (± 5)	
ADP[g]	4	1.7 (± 0.1)	26 (± 1)	15 (± 1)	
ATP[g]	4	0.57 (± 0.03)	20 (± 3)	36 (±6)	

[a] Conditions: 100 mM NaCl, 5 mM $MgCl_2$, 1 mM DTT, 20 mM HEPES (pH 7.5). [b] Calculated from the ratio of the dissociation and association rate constants. [c] Determined from association kinetics (Figures 3B and 5B). [d] Measured from time courses of mant-nucleotide release (Figures 4 and 5C). [e] Determined by equilibrium titration (Figure 2). [f] Determined by equilibrium competition (Figure 8). [g] Determined by kinetic competition (Figure 9).

Stopped-Flow Kinetics. Transient kinetic measurements were made in buffer A using an Applied Photophysics (Surrey, UK) SX.18MV-R stopped flow apparatus thermostated at the indicated temperatures (± 0.1 °C). The excitation wavelength was set to 297 nm, and fluorescence intensities at 90° were monitored through a Schott UG1 band-pass filter (tryptophan) or 400 nm long-pass colored glass filter (mant-nucleotides). Nonlinear least-squares fitting was done with Pro-K software provided with the instrument. Unless otherwise stated, uncertainties are presented as standard errors obtained from the best fits. The concentrations stated are final after mixing unless specified otherwise.

Association kinetics were measured by mixing 2 μM DbpA with a range of [mantADP] or [mantATP]. The kinetics of unlabeled ADP binding was measured by competition with mantADP by mixing DbpA with a solution of mantADP and a range unlabeled nucleotide concentrations. ATP binding kinetics were measured by competition with mantATP. MantADP dissociation was measured by rapidly mixing an equilibrated sample of DbpA (4μM before mixing) and mantADP (100 μM before mixing) with an equal volume of excess unlabeled nucleotides. Dissociation of mantATP was measured with the instrument in sequential mixing mode: DbpA (4 μM before mixing, 25% of final reaction volume) was mixed with mantATP (100 μM before mixing, 25% of final volume), aged briefly (40 ms to 1 s) then rapidly mixing with excess (4 mM, 50% of final volume) unlabeled nucleotides. The final concentrations after mixing were 1 μM DbpA, 25 μM mantATP, 2 mM MgATP, or MgADP.

Temperature Dependence of the Reaction Rates and Affinities. The temperature dependence of the kinetics was interpreted according to the transition state theory of absolute reaction rates (*18*). The activation free energy ($\Delta G^{\ddagger}$) relates to the reaction rate constant (k) according to

$$\Delta G^{\ddagger} = -RT \ln\left(\frac{kh}{k_B T}\right) = -RT \ln(K^{\ddagger}) \qquad (5)$$

where h is Planck's constant (6.63×10^{-34} J s), k_B is Boltzmann's constant (1.38×10^{-23} J K^{-1}), R is the gas constant (1.98 cal mol^{-1} K^{-1}), T is the absolute temperature in Kelvin, and $K^{\ddagger}$ is the association constant defining the equilibrium between ground and transition states. The transmission coefficient is assumed to be unity. Expanding the free energy of activation into its enthalpic ($\Delta H^{\ddagger}$) and entropic ($\Delta S^{\ddagger}$) components and rearranging yields:

$$\ln\left(\frac{kh}{k_B T}\right) = \left(\frac{-\Delta H^{\ddagger}}{R}\right)\left(\frac{1}{T}\right) + \frac{\Delta S^{\ddagger}}{R} \qquad (6)$$

permitting determination of the activation enthalpy ($\Delta H^{\ddagger}$) from the slope of the line generated by plotting the left-hand side of the relation vs inverse temperature. The intercept is not an accurate estimate of the activation entropy ($\Delta S^{\ddagger}$) since it is beyond the range of the data so it was calculated at a specific temperature from

$$\Delta S^{\ddagger} = \frac{\Delta H^{\ddagger} - \Delta G^{\ddagger}}{T} \qquad (7)$$

Nonlinear Eyring plots were fitted to an integrated form of eq 6 (see Appendix 2) that accounts for the temperature dependence of the activation enthalpy ($\Delta H^{\ddagger}$) and change in the molar heat capacity of the transition state ($\Delta C_p^{\ddagger}$):

$$\ln\left(\frac{kh}{k_B T}\right) = \ln K^{\ddagger} = \frac{\Delta S^{\ddagger}_{T_R}}{R} - \frac{\Delta H^{\ddagger}_{T_R}}{RT} + \frac{\Delta C_p^{\ddagger}}{R}\left(\ln\left(\frac{T}{T_R}\right) + \frac{T_R}{T} - 1\right) \qquad (8)$$

where the subscript r refers to values at a selected reference temperature. ($\Delta C_p^{\ddagger}$) is assumed to be constant and independent of the temperature.

The temperature dependence of the equilibrium binding affinity was analyzed using the van't Hoff form of eq 6 (linear plots) or eq 8 (curved plots) with $K^{\ddagger}$ replaced with the association equilibrium constant K_a, and the activation parameters (indicated by ‡) expressed in terms of standard heat capacity changes (ΔC_p°), and enthalpies (ΔH°) and entropies (ΔS°) of formation.

Uncertainties were propagated using the general form:

$$(df)^2 = \left[\left(\frac{\partial f}{\partial x}\right)_y^2 (dx^2) + \left(\frac{\partial f}{\partial y}\right)_x^2 (dy^2) + ...\right] \qquad (9)$$

RESULTS

All experimental measurements were made with DbpA in the absence of RNA. Under these conditions and concentrations, DbpA behaves as a noninteracting monomer as assayed by analytical ultracentrifugation and size exclusion chromatography ((*19*), unpublished data, manuscript in preparation) with a steady-state ATPase activity < 0.01 s^{-1}. The steady-state ATPase rate is activated ≥ 1000-fold by PTC−RNA to 9.7 (± 0.1) s^{-1} at 37 °C, in close agreement with published values under comparable conditions (*7*, *20*), indicating that the DbpA preparations used in this study are fully active. At 22 °C, the PTC−RNA-activated ATPase activity is 2.0 (± 0.1) s^{-1}.

Mant-Nucleotide Binding to DbpA Monitored by Fluorescence Resonance Energy Transfer. The absorption spectrum of mant-labeled nucleotides displays considerable

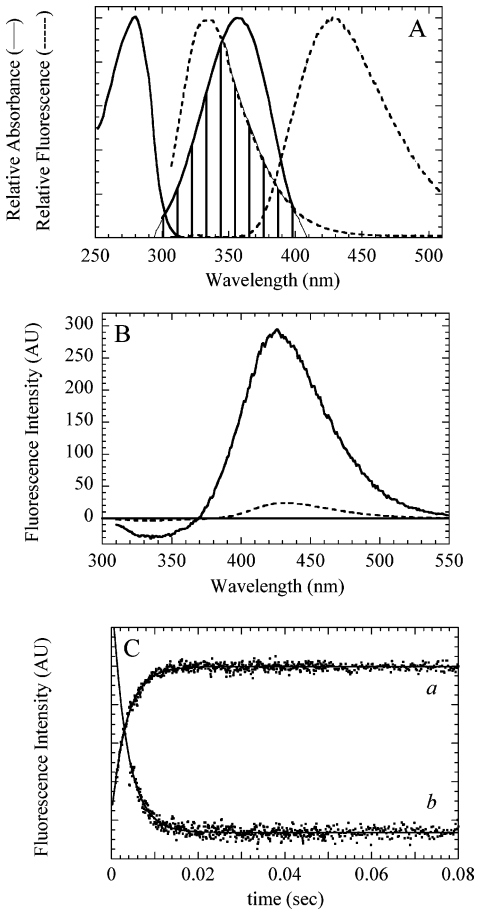

FIGURE 1: Fluorescence resonance energy transfer from DbpA tryptophans to bound mant-nucleotides. (A) Spectral overlap between the DbpA tryptophan fluorescence emission spectrum and the mant-nucleotide absorption spectrum (λ_{ex} = 297 nm). Left to right: DbpA absorption spectrum, fluorescence emission spectrum of DbpA, mant-nucleotide absorption spectrum, and fluorescence emission spectrum of mant-nucleotides. (B) Fluorescence emission difference spectra illustrating the Föster energy transfer between 2 μM DbpA and either 200 μM mantATP (dashed) or mantADP (solid). Spectra represent the difference between the observed emission of the protein−mant nucleotide complex and the predicted emission in the absence of energy transfer (e.g., the linear sum of the observed isolated emission spectra of DbpA and mant-nucleotide) and do not take into account the fraction bound. Negative regions of the spectra indicate quenching of tryptophan fluorescence, whereas positive regions of the spectra indicate enhancement of the mant fluorescence arising from energy transfer. (C) Time courses of mantADP enhancement (curve *a*) tryptophan fluorescence quenching (curve *b*) and after mixing 28 μM mantADP with 2 μM DbpA. The solid line through the tryptophan fluorescence data is the best fit to a single exponential with a rate of 289 (± 8) s^{-1}. The solid line through the mantADP fluorescence data is the best fit to a single exponential with a rate of 285 (± 7) s^{-1}. Amplitudes have been normalized for presentation. The temperature was 22 °C.

overlap with the tryptophan fluorescence emission (λ_{ex} = 297 nm) of DbpA (Figure 1A), making them good candidates for monitoring nucleotide binding through changes in fluorescence resonance energy transfer (FRET). In the presence of 200 μM mantADP, there is a significant reduction in the intrinsic tryptophan fluorescence of DbpA and an enhancement in mantADP fluorescence (Figure 1B), consistent with the presence of FRET from DbpA tryptophan(s) to bound nucleotide. Similar changes occurred in the presence of 200 μM mantATP; however, the overall amplitude changes were much smaller. Time courses of tryptophan fluorescence quenching and mantADP fluorescence enhancement follow single exponentials with similar observed rate constants (Figure 1C), suggesting that both signals are monitoring the same kinetic transition.

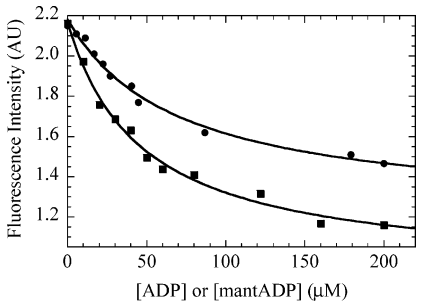

FIGURE 2: Equilibrium binding of ADP and mantADP. [ADP] (■) or [mantADP] (●) dependence of DbpA tryptophan fluorescence (λ_{ex} = 297 nm, λ_{em} = 334 nm; corrected for inner filter effects). The solid lines represent the best, unrestrained fits to a rectangular hyperbola (eq 3) yielding equilibrium binding affinities of 47 (± 6) μM for ADP and 70 (± 12) μM for mantADP binding to DbpA. The temperature was 22 °C.

Equilibrium Binding. The equilibrium binding affinity of DbpA for mantADP was measured from the nucleotide concentration dependence of tryptophan fluorescence quenching arising from FRET (Figure 2). The best fit of the data to a single-site binding model (eq 3) yields a K_d of 70 (± 14) μM for mantADP binding to DbpA (Table 1). The weak binding affinity makes it difficult to fully saturate DbpA with mantADP. The maximum fluorescence changes obtained from the best fits are 50% reduction in tryptophan fluorescence.

ADP binding generates quenching of the intrinsic DbpA tryptophan fluorescence (Figure 2, ref *8*). From the concentration dependence of tryptophan fluorescence intensity (Figure 2), the affinity of DbpA for ADP is 47 (± 6) μM (Table 1).

Because we do not know the rate or equilibrium constant for ATP hydrolysis by DbpA, equilibrium titrations with mantATP were not performed.

Mant-Nucleotide Binding Kinetics. Time courses of fluorescence enhancement after mixing DbpA with mantADP follow single exponentials (Figure 3A) with observed pseudo-first-order rate constants (k_{obs}) that depend linearly on the mantADP concentration over a broad range (Figure 3B). Transients (λ_{ex} = 366 nm, 400 nm long-pass filter) begin at the fluorescence intensity of mantADP alone (data not shown), indicating that a fast phase that generates a fluorescence change is not occurring within the dead time of our instrument. The data for mantADP binding can be modeled as a single-step, reversible bimolecular reaction (Scheme 1) with observed rate constants (k_{obs}) that depend on the rate constants and the mantADP (mD) concentration according to eq 10:

$$k_{obs} = k_{+}[\mathrm{mD}] + k_{-} \quad (10)$$

The second-order association rate constant (k_{+}) for mantADP binding to DbpA determined from the slope is 3.4 (± 0.2) μM^{-1} s^{-1} (Figure 3B). The *y*-intercept yields a dissociation rate constant (k_{-}) of 180 (± 4) s^{-1} (Figure 3B).

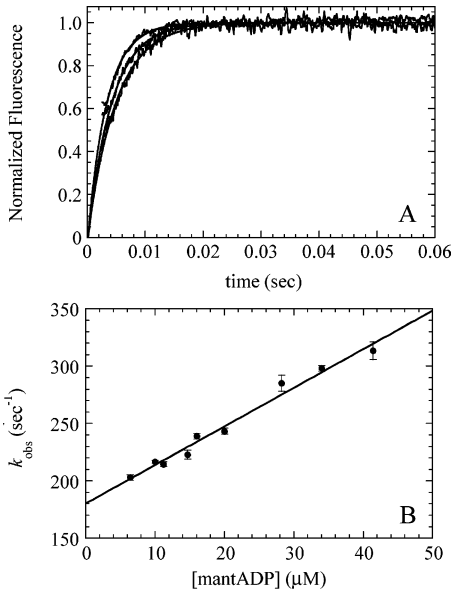

FIGURE 3: Kinetics of mantADP binding to DbpA. (A) Time courses of mantADP fluorescence change after mixing 29, 16, or 6.4 μM (left to right) mantADP with 2 μM DbpA. Data are of individual transients. Typically, 4−8 transients were averaged before fitting. The best fits to single exponentials are shown as smooth lines through the data. Amplitudes have been normalized for presentation. Each transient was scaled individually from 0 to 1. The nucleotide concentration dependence of the amplitudes is shown in the equilibrium binding titration plots (Figure 2). (B) MantADP concentration dependence of the observed rate constants. Points represent data from three different protein preparations on four separate days. Uncertainty bars represent standard errors in the fits and are contained within the points if not visible. The solid line is the best linear fit to the data. The temperature was 22 °C.

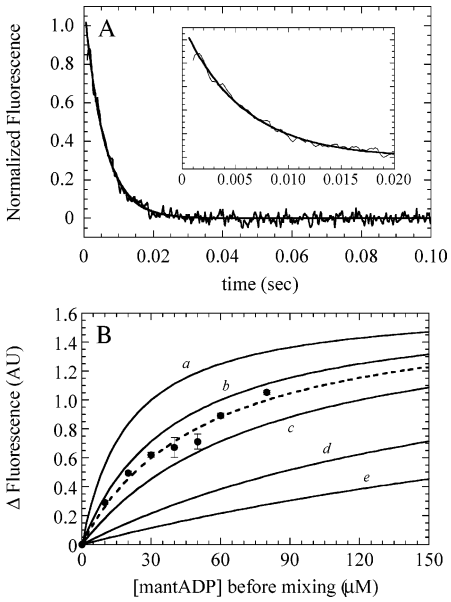

FIGURE 4: Kinetics of mantADP dissociation. (A) Time course of mantADP fluorescence change after mixing an equilibrated solution of 1.6 μM DbpA and 80 μM mantADP with 4 mM MgADP. Final concentrations after mixing are 800 nM DbpA, 2 mM MgADP, 40 μM mantADP. The smooth line is the best fit to a single exponential with a rate of 176 (± 2) s^{-1}. The inset shows the data over a 20 ms range. Fitting was constrained to data beyond 2 ms. Data are of an individual, unaveraged transient. (B) MantADP concentration dependence of the dissociation time course amplitudes. The dashed line represents the best fit to a rectangular hyperbola (eq 3) with a K_d of 54 (± 14) μM. The solid lines represent theoretical single-site binding isotherms with dissociation equilibrium constants of (*a*) 20, (*b*) 40, (*c*) 80, (*d*) 200, and (*e*) 400 μM. The temperature was 22 °C.

Scheme 1

$$\text{DbpA} + \text{mantADP} \underset{k_-}{\overset{k_+}{\rightleftharpoons}} \text{DbpA-mantADP}$$

The time course of mantADP dissociation from DbpA follows a single exponential with a rate of 176 (± 2) s^{-1} (Figure 4A), in agreement with the value estimated from the association kinetics (intercept of Figure 3B). The rate of mantADP dissociation is independent of the identity (1.5−4 mM MgATP or MgADP) of unlabeled nucleotide as expected for a unimolecular dissociation reaction with ATP and ADP competing for nucleotide binding. The amplitude of the transients depend hyperbolically on the [mantADP] before mixing, yielding a K_d of 54 (± 14) μM for the DbpA−mantADP complex (Figure 4B).

The mantADP binding affinity determined from the ratio of the association and dissociation rate constants ($K_d = k_-/k_+$) is 52 (± 3) μM, in reasonable agreement with the values obtained by equilibrium titration (70 (± 14), Figure 2, Table 1) and from the amplitudes of dissociation kinetics transients (54 (± 14), Figure 4B, Table 1).

Time courses of fluorescence change after mixing DbpA with mantATP had small amplitudes and were too rapid to measure reliably given the ~2 ms dead time of our stopped-flow (not shown).

Temperature Dependence of Mant-Nucleotide Binding Affinity and Kinetics. At low temperature (4 °C), the kinetics of mantATP binding were resolved (Figure 5A). Time courses of mantATP binding at 4 °C (Figure 5B) follow single exponentials with observed rate constants (k_{obs}) that depend linearly on the nucleotide concentration and yield an association rate constant (k_+) of 0.77 (± 0.02) μM^{-1} s^{-1} and a dissociation rate constant (k_-) of 65 (± 2) s^{-1}. At 4 °C, the dissociation rate constant measured directly by competition with excess ATP or ADP is 70 (± 4) s^{-1} (Figure 5C). The apparent affinity of DbpA for mantATP at 4 °C determined from the ratio of the rate constants is 91 (± 5) μM (Table 1).

The association rate constant for mantADP binding at 4 °C (Figure 5B) and 22 °C (Figure 3B) differ by less than a factor of 2 (Table 1). The dissociation rate constant, as estimated from the *y*-intercept, is ~3-fold slower at 4 °C (62 (± 4) s^{-1}), and in close agreement with the value measured directly from the time course of dissociation (58 (± 2) s^{-1}). DbpA binds mantADP with an affinity of 26 (± 2) μM at 4 °C (Table 1).

The energetics of nucleotide binding to DbpA were assessed from the temperature dependence of the rate and equilibrium constants (Figure 6). The association rate constant of mantADP depends little on temperature, indicative of a small activation enthalpy ($\Delta H^{\ddagger}$). An Eyring plot of the data (Figure 6A) is nonlinear, displaying a gentle, concave upward curvature suggesting an apparent change in the molar heat capacity ($\Delta C_p^{\ddagger}$) in the transition state. MantATP binding depends slightly on temperature over the range examined (4−10 °C, Figure 6A), but rapid rates and small amplitudes precluded reliable assessment of the

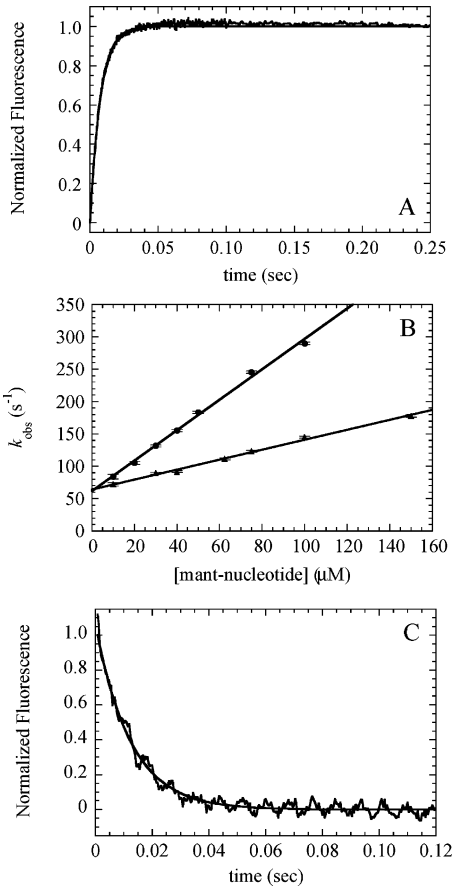

FIGURE 5: Kinetics of mant-nucleotide binding at low temperature. (A) Time course of fluorescence change after mixing 60 μM mantATP with 2 μM DbpA at 4 °C. Data represents an individual, unaveraged transient. The smooth line is the best fit to a single exponential with a rate constant of 132 s^{-1}. (B) MantADP (●) or mantATP (▲) concentration dependence of the observed rate constants. Uncertainty bars represent standard errors in the fits. (C) Time course of fluorescence change after mixing an equilibrated solution of 4 μM DbpA and 100 μM mantATP with 4 mM MgADP. Final concentrations are 2 μM DbpA, 2 mM MgADP, and 50 μM mantATP after mixing. The smooth line through the data is the best fit to a single exponential with an observed rate constant of 70 (± 4) s^{-1}. The temperature was 4 °C.

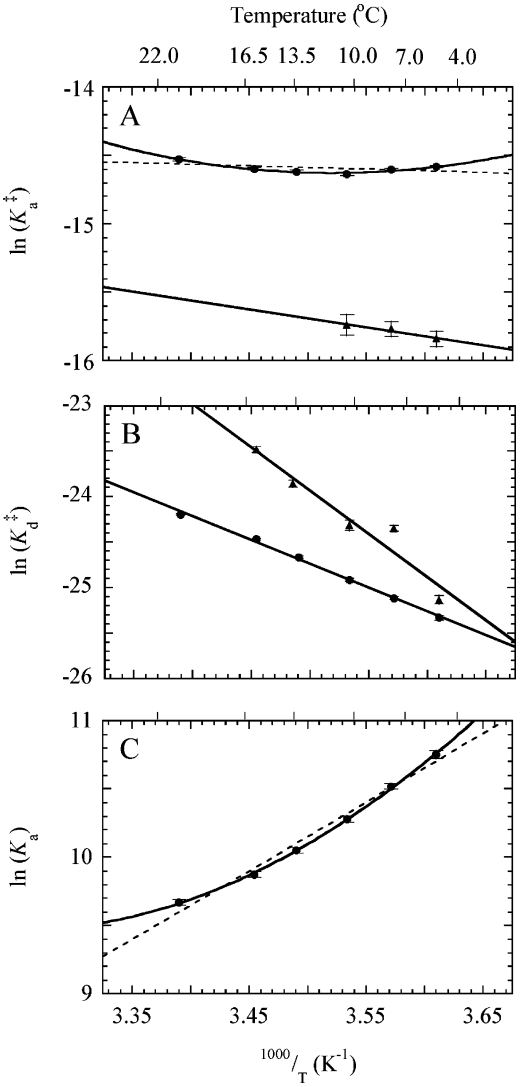

FIGURE 6: Temperature dependence of equilibrium and rate constants for nucleotide binding to DbpA. (A) Eyring plot of the second-order association rate constants for mantADP (●) or mantATP (▲) binding to DbpA. (B) Eyring plot of mantADP (●) or mantATP (▲) dissociation from DbpA. (C) van't Hoff plot of the association equilibrium constants for mantADP (●) binding to DbpA. All panels share the same *x*-axis. Note panel B ordinate is plotted on a broader scale. Nonlinear van't Hoff and Eyring plots were fitted to eqs A.2.5 and A.2.6, respectively, where ΔC_p, ΔH, and ΔS were used as fitting parameters.

curvature and consequently, extraction of thermodynamic parameters. However, given the weak temperature dependence it is clear that the activation enthalpies of both mantATP and mantADP association are small (Table 2).

Unlike the association rates, the dissociation rate constants of both nucleotides are temperature-dependent and become slower at low temperatures (Figure 6B). Dissociation of mantATP is more temperature-dependent than mantADP dissociation, indicative of a larger activation enthalpy (Table 2), presumably due to contributions from the gamma phosphate. Surprisingly, mantATP dissociation occurs with favorable entropic changes in the transition state.

Overall ADP binding occurs with an apparent positive change in heat capacity (ΔC_p° = 465 cal mol^{-1} K^{-1}, Table 2), as indicated by the curvature in the van't Hoff plot (Figure 6C).

Binding of both mantATP and mantADP to DbpA at temperatures < 22 °C occurs with large, favorable (exothermic) standard enthalpy changes ($\Delta H°$) and unfavorable (negative) entropy changes ($\Delta S°$, Figure 7, Table 2). At ≥ 22 °C, ADP binding is endothermic and occurs with favorable entropy changes (Figure 7). Therefore, at physiological temperatures ADP binding is driven by favorable entropic contributions.

Since the change in entropy contributes significantly to the energetics of ADP binding at physiological temperatures, the entropic change upon binding ADP was analyzed in more detail. The overall change in entropy ($\Delta S°$) for protein−ligand interactions is the sum of various contributions and can be expressed as

$$\Delta S° = \Delta S°_{HE} + \Delta S°_{rt} + \Delta S°_{other} \qquad (11)$$

where $\Delta S°_{HE}$ corresponds to entropy changes arising from the hydrophobic effect, $\Delta S°_{rt}$ reflects changes in rotational and translational entropy of the molecules, and $\Delta S°_{other}$ accounts for all other entropy changes such as substrate-induced structural reorganization, which are assumed to be temperature-independent (*21*).

Table 2: Thermodynamic Parameters for Mant Nucleotides Binding to DbpA

parameter[a]	mantADP, 4 °C	mantATP, 4 °C	mantADP, 22 °C
$\Delta G_a^{\ddagger}$ (kcal mol^{-1})[b]	8.0 (± 0.1)	8.7 (± 0.1)	8.5 (± 0.1)
$\Delta H_a^{\ddagger}$ (kcal mol^{-1})	−2.0 (± 0.4)[c]	2.6 (± 0.6)[d]	3.1 (± 0.4)[c]
$\Delta S_a^{\ddagger}$ (kcal mol^{-1})	−36.0 (± 1.3)[c]	−21.9 (± 2.3)[e]	−18.4 (± 1.3)[c]
$-T\Delta S_a^{\ddagger}$ (kcal mol^{-1})	10.0 (± 0.4)	6.1 (± 0.3)	5.4 (± 0.4)
$\Delta C_p^{\ddagger}$ (kcal mol^{-1} K^{-1})	0.28 (± 0.04)[c]		0.28 (± 0.04)[c]
$E_{act,a}$ (kcal mol^{-1})[f]	−1.5 (± 0.4)	3.2 (± 0.6)	3.7 (± 0.4)
$\Delta G_d^{\ddagger}$ (kcal mol^{-1})[b]	13.9 (± 0.1)	13.8 (± 0.4)	14.1 (± 0.1)
$\Delta H_d^{\ddagger}$ (kcal mol^{-1})[d]	10.4 (± 0.4)	18.8 (± 2.9)	10.4 (± 0.3)
$\Delta S_c^{\ddagger}$ (cal mol^{-1}K^{-1})[d]	−12.6 (± 1.1)	17.9 (± 10.2)	−12.6 (± 1.1)
$-T\Delta S_d^{\ddagger}$ (kcal mol^{-1})	3.5 (± 0.3)	−5.0 (± 2.8)	3.7 (± 0.3)
$E_{act,d}$ (kcal mol^{-1})[f]	11.0 (± 0.3)	19.4 (± 2.9)	11.0 (± 0.3)
ΔG_{app}° (kcal mol^{-1})[g]	−5.9 (± 0.1)	−5.1 (± 0.1)	−5.7 (± 0.1)
ΔH_{app}° (kcal mol^{-1})	−14.0 (± 1.5)[h]	−16.2 (± 3.0)[i]	−5.7 (± 0.1)[h]
ΔS_{app}° (cal mol^{-1} K^{-1})	−29.0 (± 2.0)[h]	−39.9 (± 10.5)[i]	∼ 0[h]
$-T\Delta S_{app}^{\circ}$ (kcal mol^{-1})	8.0 (± 0.6)	11.0 (± 2.9)	∼ 0
ΔC_p° (kcal mol^{-1} K^{-1})	0.47 (± 0.05)[h]		0.47 (± 0.05)[h]

[a] Subscripts a and d refer to association and dissociation reactions, respectively. [b] Calculated from eq 5. [c] Calculated from eq 8. [d] Calculated from eq 6. [e] Calculated from eq 7. [f] Calculated from $E_{act} = \Delta H^{\ddagger} + RT$. [g] Calculated from $\Delta G_{app}^{\circ} = \Delta G_a^{\ddagger} - \Delta G_d^{\ddagger} = RT \ln(K_d^{kin})$. [h] Calculated from the van't Hoff form of eq 8. [i] Calculated from $\Delta H_{app}^{\circ} = \Delta H_a^{\ddagger} - \Delta H_d^{\ddagger}$, $\Delta S_{app}^{\circ} = \Delta S_a^{\ddagger} - \Delta S_d^{\ddagger}$.

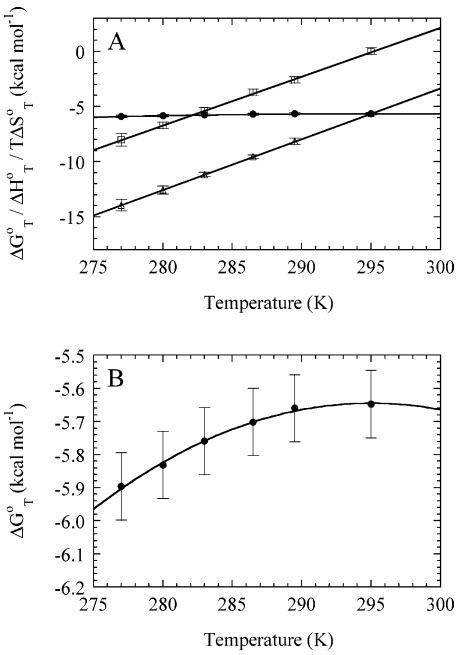

FIGURE 7: Thermodynamic contributions to the free energy of mantADP binding to DbpA. (A) Temperature dependence of changes in enthalpy (ΔH°, Δ), entropy ($T\Delta S^{\circ}$, □) and Gibbs free energy (ΔG°, ●) occurring with mantADP binding to DbpA. (B) Inset of panel A. Error bars reflect uncertainties in ΔC_p, ΔH°, and ΔS°. ΔH°, and ΔS° were calculated using eqs A.2.2 and A.2.3, respectively.

Contributions arising from ΔS_{other}° are usually very small for rigid-body associations, where ΔS° is determined by the magnitudes of ΔS_{HE}° and ΔS_{rt}° (*21*). However, for an induced-fit mechanism, a significant value of ΔS_{other}° reflects changes in conformational entropy on complex formation (*21*). The ΔS_{HE}° for mantADP binding to DbpA at 22 °C (where $\Delta S^{\circ} = 0$; Figure 7; Table 2) is[2] −169 cal mol^{-1} K^{-1}. Because ΔS_{rt}° is relatively constant and averages to be about −50 cal mol^{-1} K^{-1} for typical protein−ligand associations

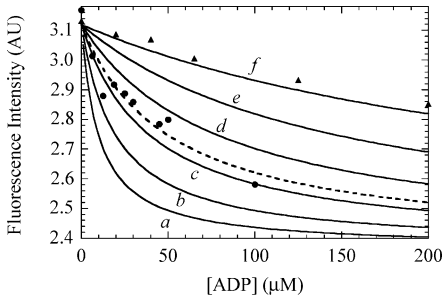

FIGURE 8: ADP and ATP binding affinities measured by competition with mantADP. ADP (●) and ATP (▲) concentration dependence of the DbpA-mantADP fluorescence (λ_{ex} = 297 nm, λ_{em} = 443 nm; corrected for inner filter effects). The solid lines represent theoretical single-site binding isotherms with dissociation equilibrium constants of (*a*) 20, (*b*) 40, (*c*) 60, (*d*) 80, (*e*) 140, and (*f*) 400 μM. The dashed line represents the best fit to eq 4 with a K_d of 70 (± 25) μM. The temperature was 22 °C.

(*21*), summation of these two contributions leaves a substantial favorable ΔS_{other}° term of 219 cal mol^{-1} K^{-1}. This value for ΔS_{other}° falls within the midrange of values reported for processes that couple local or long-range folding to site-specific binding (*21*). Thus, the significant value of ΔS_{other}° is consistent with a conformational change in DbpA occurring with ADP binding. The positive value suggests an increase in the number or amplitudes of conformational motions may be the source of ΔS_{other}°. The number of amino acid residues (*R*) that change their conformation can be estimated from

$$R = \frac{\Delta S_{other}^{\circ}}{5.5 \text{ cal mol}^{-1} \text{ K}^{-1}} \qquad (12)$$

assuming that ΔS_{other}° arises entirely from changes in conformational entropy (*21*). Our calculations predict that ∼40 residues change their conformation when ADP binds, suggesting that the DbpA conformational change may be global in nature and not limited to the nucleotide binding residues.

Equilibrium Binding of Unlabeled Nucleotides Measured by Competition. The affinity of ADP for DbpA at 22 °C measured by equilibrium competition (Figure 7) is 70.2 (± 25.3) μM, comparable to mantADP, indicating that the mant modification does not disrupt equilibrium binding. ATP binds more weakly with a K_d > 100 μM (estimated ∼400 μM, Figure 8).

Kinetics of Unlabeled Nucleotides Measured by Competition. The kinetics and affinity of unlabeled nucleotide were measured by competition with mant nucleotides (*24*) and analyzed according to Scheme 2, which describes competitive binding of mant nucleotide (M) and unlabeled nucleotide (U) to a single DbpA binding site where * denotes the high fluorescence state and $K_D = k_{-D}/k_{+D}$ (Scheme 2).

[2] Calculated from $\Delta S_{HE}^{\circ} = 1.35\Delta C_p(\ln T/386)$, which assumes the ΔC_p° arises entirely from changes in the hydrophobic effect (*22*). While this is an oversimplification and ignores contributions to ΔC_p° arising from specific-ion binding, which can often, but not always (*23*), be significant, it provides a foundation for interpreting the contributions to ΔC_p° based on analogy to well-established systems and established thermodynamic formalisms. Furthermore, the weak ionic strength dependence of the mantADP binding affinity (less than 3-fold difference between 0.05 and 0.4 M NaCl, MAT, and EMDLC, unpublished observations) suggests this is a reasonable first approximation.

Scheme 2

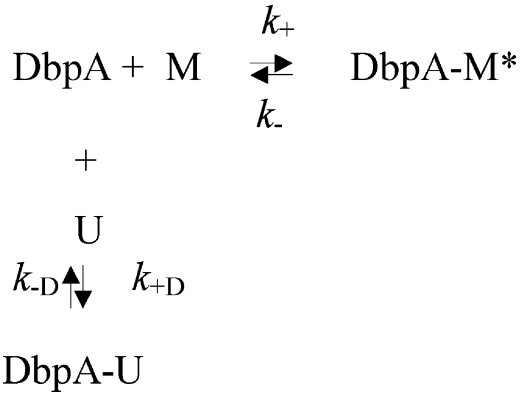

For such a reversible reaction mechanism, the observed pseudo-first-order rate constants (k_{obs}) of the time courses of fluorescence enhancement after rapidly mixing DbpA with mantADP or a mixture of mantADP and unlabeled nucleotide (i.e., ADP) depend on the sum of the rate constants for nucleotide binding and concentrations according to (*25*−*27*):

$$k_{obs} = k_{+D}[D] + k_{-D} + k_{+}[mD] + k_{-} \qquad (13)$$

permitting determination of the rate constants of unlabeled nucleotide binding from the slope and intercept of the line generated from plotting k_{obs} vs [ADP].

The time course of fluorescence enhancement after mixing 35 μM mantADP with DbpA at 4 °C follows a single exponential (Figure 3) with an observed pseudo-first-order rate constant ($k_{obs} = k_{+}[mD] + k_{-}$) of 134 s^{-1} (Figure 9, filled square). When a solution of ADP and mantADP is mixed with DbpA, time courses follow single exponentials with observed rate constants that depend linearly on the [ADP] (Figure 9). The slope yields an association rate constant for ADP binding (k_{+D} = 1.7 μM^{-1} s^{-1}). The intercept (160 s^{-1}) is proportional to the sum of the observed rate constants for mantADP binding and ADP dissociation ($k_{+}[mD] + k_{-} + k_{-D}$, Scheme 1, eq 13). A dissociation rate constant of ADP (k_{-D}) of 26 s^{-1} was calculated from the difference of the observed rates in the absence of ADP and the intercept from the best fit of the [ADP] dependence (Figure 9). The affinity calculated from the ratio of the rate constants is 15 (± 1) μM at 4 °C (Table 1).

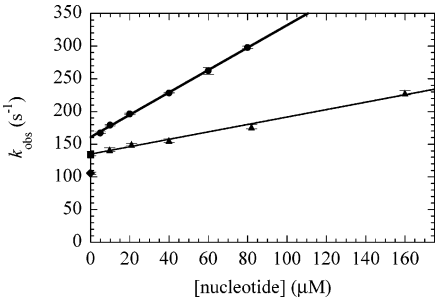

FIGURE 9: ADP and ATP binding measured by kinetic competition with mantADP. [ADP] dependence of the observed rate constant for 30 μM mantADP binding to DbpA (●); (■) represents the observed rate constant for mantADP binding in the absence of ADP. [ATP] dependence of the observed rate constant for 30 μM mantATP binding to DbpA (▲); (◆) represents the observed rate constant of mantATP binding in the absence of ATP. The solid line is the best fit of the data acquired in the presence of competing ADP. The temperature was 4 °C.

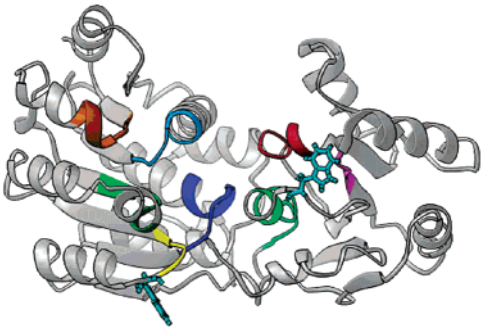

FIGURE 10: Structural homology model of the DbpA helicase core. The core model has an approximate width of 65 Å. Tryptophans 187 (lower left) and 320 (upper right) are colored aqua blue. The P-loop/Walker A motif (motif I) is colored dark blue, and the DEAD-box/Walker B motif (motif II, to the left of the P-loop) is colored bright green. The nucleotide is predicted to bind in the small cleft between the DEAD-box and P-loop. Other conserved helicases motifs are domains Ia (bright blue), Ib (orange), III/SAT motif (yellow), IV (magenta), V (red), and VI (dark green) are shown for clarity. Figure adapted from Henn et al. (*8*) and generated using the program Ribbons (*48*).

Similar kinetic measurements in which ATP was competed with mantATP (Figure 9) yield a second-order association rate constant of 0.57 μM^{-1} s^{-1}, a dissociation rate constant of 20 s^{-1}, and an equilibrium binding affinity of 36 μM (Table 1).

DISCUSSION

Tryptophan-Mant Fluorescence Resonance Energy Transfer (FRET). Mant-nucleotide binding to DbpA generates FRET from DbpA tryptophans to the mant moiety of the bound nucleotide (Figure 1). DbpA contains four tryptophan residues: W187, W320, W366, and W438. Structural homology modeling of the helicase core of DbpA (*8*) suggests that W187 and W320 are within ~18−20 Å of the presumed nucleotide binding site (Walker A and B motifs) and could potentially contribute to the observed FRET (Figure 10). W366 and W438 are found in the C-terminal extension of DbpA. The Föster distance for tryptophans can be as large as 40 Å (*28*), which is smaller than the core domain dimensions imposed by structural homology modeling (*8*) and the Stokes radius of DbpA (*19*). Although tryptophan residues in the core are the most likely donors, without any further information regarding the orientation of the residues with respect to the bound nucleotide and fluorophore assigning the observed FRET to a specific tryptophan or conformation of DbpA is not possible. However, the observed FRET differences between mantATP and mantADP provide insight into the nucleotide-dependent conformation of DbpA.

Although DbpA has four tryptophan residues, a transfer efficiency (E) was calculated assuming a single tryptophan donor and no intermolecular contributions to energy transfer (*28*) using the following relationship (*29*):

$$E = \left[\frac{F(297nm)}{F(340nm)} - \frac{\epsilon_{mantD}(297nm)}{\epsilon_{mantD}(340nm)}\right] \cdot \left[\frac{\epsilon_{mantD}(340nm)}{\epsilon_{DbpA}(297nm)}\right] \qquad (14)$$

where F is the corrected fluorescence intensities and ϵ is the molar extinction coefficients of mantADP or DbpA at the indicated wavelengths. An 80% energy transfer efficiency

Scheme 3

$$P + N \underset{k_{-1}}{\overset{k_{+1}}{\rightleftharpoons}} (PN) \underset{k_{-2}}{\overset{k_{+2}}{\rightleftharpoons}} PN^*$$

is achieved with mantADP binding to DbpA, whereas a 50% efficiency is observed for mantATP. The different FRET efficiencies suggest that DbpA adopts different conformations depending on the bound nucleotide. The lower FRET efficiency with mantATP may result from a subsequent conformational change, such as hydrolysis, and depopulation of the high fluorescence states. Alternatively, ADP binding may be coupled to conformational rearrangement of DbpA promoting a higher energy transfer state. By limited proteolysis, binding of ADP alters the conformation of DbpA (*8*), consistent with such a mechanism.

Kinetic Mechanism of Nucleotide Binding to DbpA. While there have been previous kinetic measurements of nucleotide binding to DNA and RNA helicases (*30*−*32*), to our knowledge this is the first transient kinetic analysis of nucleotide binding to a DEAD-box RNA helicase. Our results demonstrate that ATP and ADP binding to DbpA are far more rapid than the steady-state ATPase rate of DbpA in the absence of RNA ($<0.01\ s^{-1}$), indicating that nucleotide binding and dissociation do not limit the overall ATPase cycle. ATP hydrolysis, P_i release, or a conformational change preceding these transitions must therefore limit the DbpA turnover rate. It is likely that RNA activates the ATPase activity of DbpA by accelerating rate-limiting hydrolysis or P_i release.

ATP binds DbpA more weakly than does ADP (Table 1). Under physiological nucleotide concentrations of ∼3 mM MgATP and ∼600 μM MgADP (*33*), we expect approximately equal partitioning into ADP- and ATP-bound states in the absence of PTC−RNA. The weak ATP affinity presumably accounts for the inability of low (micromolar) ATPγS concentrations to alter the intrinsic fluorescence or proteolysis of DbpA (*8*). The affinity for ATP measured in this study is significantly weaker than the affinity reported using a direct binding assay (*34*). The higher affinity measured by direct binding may due to population of ATP- and ADP-P_i-bound states, yielding a higher apparent affinity for ATP binding.

Nucleotide binding to DbpA can be modeled as simple, one-step reversible binding mechanisms (Scheme 1). Nucleotide binding to most characterized NTPases and molecular motors (*35*) occurs via (at least) a two-step reaction mechanism (Scheme 3) where (PN) is a collision complex in a weak, rapid equilibrium with free nucleotide (N) that isomerizes to a high fluorescent state (indicated by *) with high nucleotide affinity. Although it is likely that nucleotide binding to DbpA follows a similar mechanism, our measurements could not identify two-step nucleotide binding to DbpA (i.e., hyperbolic concentration dependence of k_{obs}, Figures 3B, 5B, and 8), presumably because the equilibrium constant for initial binding is weak ($k_{-1}/k_{+1} > 20\ \mu M$) and the maximum rate ($k_{+2} + k_{-2}$) > 350 s^{-1} under all conditions examined.

The *E. coli* DNA helicase Rep binds nucleotides via a two-step mechanism with two high fluorescence intermediates linked by a slow isomerization that generates complex biphasic time courses of nucleotide binding (*32*). DnaB also populates multiple high-fluorescence states and displays multiphasic kinetics (*30*). The lack of significant deviation from simple exponential behavior suggests that DbpA populates only a single high fluorescence state or that the isomerization rate constant is very rapid ($k_{+2} + k_{-2} \gg k_{+1} + k_{-1}$).

The second-order association rate constants for nucleotide binding to DbpA have low activation energies ($E_{act} = \Delta H_a^{\ddagger} + RT = 1-3$ kcal mol^{-1}; Table 2) relative to the predicted activation energy of a diffusion-limited reaction in water (∼4−5 kcal mol^{-1}; ref *36*). However, the rate constants are approximately 3 orders of magnitude lower than the theoretical maximum ($\sim 3 \times 10^9\ M^{-1}\ s^{-1}$) for the diffusion-limited collision of two uncharged, uniformly reactive spheres as defined by Smoluchowski[3] (*37*). Association rate constants that are considerably slower than the diffusion-limit often arise because binding occurs via a two-step reaction mechanism (Scheme 2) with an inherently weak collision complex (*38*). If nucleotide binding to DbpA follows a similar mechanism, the absence of curvature in k_{obs} vs [mN] (Figure 3B) indicates that the affinity for the collision complex would be >20 μM, which is much weaker than the affinity formed upon initial encounter with other characterized helicases (*32*).

Energetics of Nucleotide Binding to DbpA. Both mantADP and mantATP bind DbpA with relatively weak affinities (Table 1) and display favorable enthalpic (exothermic $\Delta H°$) and unfavorable entropic (negative $\Delta S°$) contributions to the free energy of binding ($\Delta G°$) at low temperatures (<22 °C, Table 2). At physiological temperatures (>22 °C), ADP binding occurs with favorable entropy changes (positive $\Delta S°$; Figure 7). Nonlinear Eyring and van't Hoff plots for mantADP binding (Figure 6) indicate that a change in the heat capacity ($\Delta C_p°$) of the system occurs with ADP binding to DbpA. We could not examine mantATP binding over a similar temperature range due to rapid rates, weak binding affinity, and consequently a small signal.

While it is difficult to assign the factors that contribute to changes in heat capacity, which may include contributions from DbpA, nucleotide, ions, and solvent, several interpretations can be made based on comparison with well-characterized systems (*32*). The change in heat capacity ($\Delta C_p°$) suggests that DbpA undergoes a structural reorganization upon ADP binding, consistent with a multistep binding mechanism (Scheme 3) and limited proteolysis studies (*8*). The fact that $\Delta C_p°$ is positive reveals important insight into the types of conformational changes that may occur. Although most characterized protein−ligand interactions that display a change in heat capacity occur with a negative $\Delta C_p°$ values, several cases of positive $\Delta C_p°$ have been identified

[3] $k_{collision} = [4\pi N_A(D_P + D_N)(r_P + r_N)]/1000$, where N_A is Avogadro's number, D_P and D_N are the diffusion coefficients of the protein and the nucleotide, respectively, and r_P and r_N are their interaction radii. The diffusion coefficient of DbpA (D_P) determined by sedimentation velocity is $6.6 \times 10^{-7}\ cm^2\ s^{-1}$ (*19*). The diffusion coefficients of mant-nucleotides ($D_N = 3.42 \times 10^{-6}\ cm^2/s$) were calculated from the rotational correlation time of Mn-ATP (*37*), which agrees with values calculated from the fluorescence lifetimes and anisotropies (*30*). The interaction radii have been taken as equal to the approximate size of the radius of the nucleotide, $r_N = r_P \approx 4.8$ Å. Accounting for steric constraints and non-uniform reactive surfaces is expected to lower the $k_{collision}$ by approximately an order of magnitude (*37*).

(*39*−*41*). A positive ΔC_p° is often attributed to solvent exposure of an enlarged hydrophobic protein surface (*21*, *42*), suggesting that ADP binding induces a conformational change in DbpA that exposes hydrophobic residues to the solvent, perhaps mediating favorable base stacking interactions with bound RNA. However, such a mechanism is expected to yield negative ΔS° values at room temperature (*42*). Transfer of polar residues to a non-polar environment (*43*), charge neutralization, and order-to-disorder transitions involving weakly interacting components (*44*) can also generate a positive ΔC_p°. The positive ΔC_p° and ΔS° may therefore also reflect contributions from coordination of bound ADP as well as an increase in the number of soft internal modes and isoenergetic conformations of DbpA.

Negligible values of ΔS°_{other} are expected for rigid-body interactions, while interactions that are coupled to conformational rearrangement show large ΔS°_{other} values (*21*). The favorable entropic changes (ΔS°) for mantADP binding at physiological temperatures and the magnitude of ΔS°_{other} are consistent with increased conformational flexibility and/or amplitude of harmonic motions being coupled to ADP binding. Although the regions undergoing these changes may occur anywhere in DbpA, they are most likely to be dominated by the flexible loops that define the nucleotide binding site (i.e., Walker A and Walker B motif), as indicated by changes in proteolysis occurring at the residues within and surrounding the P-loop/Walker A motif (*8*).

Structural Dynamics of the P-Loop/Walker A Motif. Among DNA and RNA helicases, structural and phylogenetic comparisons suggest the core domains of DEAD-box proteins adopt very similar three-dimensional conformations and that the conserved signature motifs within these domains are positioned nearly identical (*45*). Residues comprising the P-loop/Walker A motif of DNA and RNA helicases are thought to coordinate the bound nucleotide and cation (*45*). In the absence of bound ligands (i.e., nucleotide and nucleic acid), the P-loop/Walker A motif in the structures of DNA helicases (Rep and PcrA) have always been observed in an "open" conformation that makes the nucleotide binding site accessible to the solvent and therefore conducive to nucleotide binding (*46*, *47*). The open conformation is also observed in structures with bound nucleotides (*46*, *47*). However, the structures of the DEAD-box RNA helicases, eIF4A and BstDEAD show closed conformations of the P-loop in the absence of bound nucleotide (*46*, *47*).

The slower than diffusion-limited association rate constants, low activation energies, and heat capacity changes may reflect conformational dynamics of the P-loop that interfere with productive nucleotide binding. ATP binds more weakly and with a lower association rate constant than ADP, indicating that accommodating the gamma phosphate of ATP is difficult and dictates the relative binding affinities ADP and ATP.

ACKNOWLEDGMENT

We thank Drs. Irit Sagi (Weizmann Institute of Science, Rehovot, Israel) for providing the plasmid encoding DbpA and Arnon Henn for stimulating discussions.

APPENDIX 1

Stoichiometric binding of labeled nucleotide (e.g., mantADP, mD) and unlabeled nucleotide (U) to DbpA (P) can be described by the following reversible equilibrium reactions:

$$P + mD \rightleftharpoons^{K_{mD}} PmD \quad \text{(A1.1)}$$

$$P + U \rightleftharpoons^{K_U} PU \quad \text{(A1.2)}$$

where the dissociation equilibrium constants, K_{mD} and K_U are defined by the free (F) and total (T) reactant concentrations according to

$$K_{mD} = \frac{[P]_F[mD]_F}{[PmD]} = \frac{([P]_T - [PmD] - [PU])([mD]_T - [PmD])}{[PmD]} \quad \text{(A1.3)}$$

$$K_U = \frac{[P]_F[U]_F}{[PU]} = \frac{([P]_T - [PmD] - [PU])([U]_T - [PU])}{[PU]} \quad \text{(A1.4)}$$

Expressing eqs A1.3 and A1.4 in terms of their ratio gives:

$$\frac{K_{mD}}{K_U} = \frac{([mD]_T - [PmD])[PU]}{([U]_T - [PU])[PmD]} \quad \text{(A1.5)}$$

Rearranging and isolating [PU] yields:

$$K_{mD}[U]_T[PmD] = [PU](K_U[mD]_T - K_U[PmD] + K_{mD}[PmD]) \quad \text{(A1.6)}$$

If we define

$$\Delta K = K_{mD} - K_U \quad \text{(A1.7)}$$

then

$$K_{mD}[U]_T[PmD] = [PU](K_U[mD]_T + \Delta K[PmD]) \quad \text{(A1.8)}$$

and

$$[PU] = \frac{K_{mD}[U]_T[PmD]}{K_U[mD]_T + \Delta K[PmD]} \quad \text{(A1.9)}$$

Substituting eq A1.9 for [PU] in eq A1.3 yields

$$K_{mD} = \frac{\left([P]_T - [PmD] - \left[\frac{K_{mD}[U]_T[PmD]}{K_U[mD]_T + \Delta K[PmD]}\right]\right)([mD]_T - [PmD])}{[PmD]} \quad \text{(A.10)}$$

which can be rearranged to

$$K_{mD}[PmD] = [P]_T[mD]_T - [PmD][mD]_T - \left[\frac{K_{mD}[U]_T[PmD][mD]_T}{K_U[mD]_T + \Delta K[PmD]}\right] - [P]_T[PmD] + [PmD]^2 + \left[\frac{K_{mD}[U]_T[PmD]^2}{K_U[mD]_T + \Delta K[PmD]}\right] \quad \text{(A1.11)}$$

Multiplying both sides of the equation by (K_U[mD]$_T$ + ΔK[PmD]) generates

$$K_U[\mathrm{mD}]_T K_U[\mathrm{PmD}] + K_{mD}\Delta K[\mathrm{PmD}]^2 = [\mathrm{P}]_T[\mathrm{mD}]_T{}^2 K_U + [\mathrm{P}]_T[\mathrm{mD}]_T[\mathrm{PmD}]\Delta K - K_{mD}[\mathrm{U}]_T[\mathrm{PmD}][\mathrm{mD}]_T - [\mathrm{P}]_T[\mathrm{PmD}]K_U[\mathrm{mD}]_T - [\mathrm{P}]_T\Delta K[\mathrm{PmD}]^2 + K_U[\mathrm{mD}]_T[\mathrm{PmD}]^2 + \Delta K[\mathrm{PmD}]^3 + K_{mD}[\mathrm{U}]_T[\mathrm{PmD}]^2 \quad (A1.12)$$

Collecting coefficients of [PmD] and rewriting by collecting common factors yields

$$\Delta K[\mathrm{PmD}]^3 + (K_U[\mathrm{mD}]_T + K_{mD}[\mathrm{U}]_T - \Delta K([\mathrm{P}]_T + [\mathrm{mD}]_T + K_{mD}))[\mathrm{PmD}]^2 + [\mathrm{mD}]_T([\mathrm{P}]_T\Delta K - [\mathrm{mD}]_T K_U - K_{mD}[\mathrm{U}]_T - [\mathrm{P}]_T K_U - K_U K_{mD})[\mathrm{PmD}] + [\mathrm{P}]_T[\mathrm{mD}]_T{}^2 K_U = 0 \quad (A1.13)$$

Dividing by ΔK generates the expression:

$$[\mathrm{PmD}]^3 + \frac{K_U[\mathrm{mD}]_T + K_{mD}[\mathrm{U}]_T - \Delta K([\mathrm{P}]_T + [\mathrm{mD}]_T + K_{mD})}{\Delta K} \times [\mathrm{PmD}]^2 + \frac{[\mathrm{mD}]_T([\mathrm{P}]_T\Delta K - [\mathrm{mD}]_T K_U - K_{mD}[\mathrm{U}]_T - [\mathrm{P}]_T K_U - K_U K_{mD})}{\Delta K} \times [\mathrm{PmD}] + \frac{[\mathrm{P}]_T[\mathrm{mD}]_T{}^2 K_U}{\Delta K} = 0 \quad (A1.14)$$

which is a cubic equation of the form $x^3 + ax^2 + bx + c = 0$, where

$$a = \frac{K_U[\mathrm{mD}]_T + K_{mD}[\mathrm{U}]_T - \Delta K([\mathrm{P}]_T + [\mathrm{mD}]_T + K_{mD})}{\Delta K}$$

$$b = \frac{[\mathrm{mD}]_T([\mathrm{P}]_T\Delta K - [\mathrm{mD}]_T K_U - K_{mD}[\mathrm{U}]_T - [\mathrm{P}]_T K_U - K_U K_{mD})}{\Delta K}$$

and

$$c = \frac{[\mathrm{P}]_T[\mathrm{mD}]_T{}^2 K_U}{\Delta K} \quad (A1.15)$$

and roots defined by:

$$[\mathrm{PmD}] = -2\sqrt{Q}\cos\left(\frac{\theta}{3}\right) - \frac{a}{3} \quad (A1.16)$$

when $K_U > K_{mD}$, and

$$[\mathrm{PmD}] = -2\sqrt{Q}\cos\left(\frac{\theta + 4\pi}{3}\right) - \frac{a}{3} \quad (A1.17)$$

when $K_U < K_{mD}$, where

$$\theta = \cos^{-1}\left(\frac{R}{\sqrt{Q^3}}\right) \quad (A1.18)$$

$$Q = \frac{a^2 - 3b}{9} \quad (A1.19)$$

and

$$R = \frac{2a^3 - 9ab + 27c}{54} \quad (A1.20)$$

In the case when $K_{mD} = K_U$, equation A5 simplifies to

$$\frac{[\mathrm{PmD}]}{[\mathrm{PU}]}K_{mD} = \frac{[\mathrm{mD}]_T}{[\mathrm{U}]_T}K_U \quad (A1.21)$$

so the ratio of bound ligands is equal to the ratio of their total concentrations:

$$\frac{[\mathrm{PmD}]}{[\mathrm{PU}]} = \frac{[\mathrm{mD}]_T}{[\mathrm{U}]_T} \quad (A1.22)$$

APPENDIX 2

The thermodynamic parameters $\Delta H°$ (enthalpy change), $\Delta S°$ (entropy change), and $\Delta C_p°$ (heat-capacity change) for nucleotide binding to DbpA were calculated at a given temperature (T) from standard thermodynamic relationships:

$$\Delta G_T° = \Delta H_T° - T\Delta S_T° \quad (A2.1)$$

$$\Delta H_T° = \Delta H_{T_R}° + \Delta C_p° \int_{T_R}^{T} dT = \Delta H_{T_R}° + \Delta C_p°(T - T_R) \quad (A2.2)$$

$$\Delta S_T° = \Delta S_{T_R}° + \Delta C_p° \int_{T_R}^{T} \frac{dT}{T} = \Delta S_{T_R}° + \Delta C_p° \ln\left(\frac{T}{T_R}\right) \quad (A2.3)$$

where T_R is a reference temperature, here taken to be 277 K. The value $\Delta C_p°$ is assumed to be constant and independent of temperature. Combining equations A2.1−A2.3 yields

$$\Delta G_T° = \Delta H_{T_R}° + \Delta C_p°(T - T_R) - T\Delta S_{T_R}° - T\Delta C_p° \ln(T/T_R) \quad (A2.4)$$

which, by making use of $\Delta G° = -RT \ln K$, can be rearranged to

$$\ln K = \frac{\Delta S_{T_R}°}{R} - \frac{\Delta H_{T_R}°}{RT} + \frac{\Delta C_p°}{R}\left(\ln\left(\frac{T}{T_R}\right) + \frac{T_R}{T} - 1\right) \quad (A2.5)$$

where K is the association equilibrium constant for nucleotide binding ($K = k_+/k_-$). Equation A2.5 can be expressed in terms of Eyring activation parameters (indicated by ‡) and rate constants to account for changes that occur when going from ground states to transition states:

$$\ln\left(\frac{kh}{k_B T}\right) = \ln K^‡ = \frac{\Delta S^‡_{T_R}}{R} - \frac{\Delta H^‡_{T_R}}{RT} + \frac{\Delta C^‡_p}{R}\left(\ln\left(\frac{T}{T_R}\right) + \frac{T_R}{T} - 1\right) \quad (A2.6)$$

REFERENCES

1. Linder, P., Lasko, P. F., Ashburner, M., Leroy, P., Nielsen, P. J., Nishi, K., Schnier, J., and Slonimski, P. P. (1989) Birth of the D-E-A-D box, *Nature 337*, 121−122.
2. Henn, A., Medalia, O., Shi, H. P., Steinberg, M., Franceschi, F., and Sagi, I. (2001) Visualization of unwinding activity of duplex RNA by DbpA, a DEAD box helicase, at single-molecule

resolution by atomic force microscopy, *Proc. Natl. Acad. Sci., U.S.A. 98*, 5007−5012.
3. Jankowsky, E., Gross, C. H., Shuman, S., and Pyle, A. M. (2001) Active disruption of an RNA-protein interaction by a DExH/D RNA helicase, *Science 291*, 121−125.
4. Mohr, S., Stryker, J. M., and Lambowitz, A. M. (2002) A DEAD-box protein functions as an ATP-dependent RNA chaperone in group I intron splicing, *Cell 109*, 769−779.
5. Rocak, S., and Linder, P. (2004) Dead-box proteins: The driving forces behind RNA metabolism, *Nat. Rev. Mol. Cell Biol. 5*, 232−241.
6. Rogers, G. W., Jr., Richter, N. J., Lima, W. F., and Merrick, W. C. (2001) Modulation of the helicase activity of eIF4A by eIF4B, eIF4H, and eIF4F, *J. Biol. Chem. 19*, 19.
7. Tsu, C. A., and Uhlenbeck, O. C. (1998) Kinetic analysis of the RNA-dependent adenosinetriphosphatase activity of DbpA, an *Escherichia coli* DEAD protein specific for 23S ribosomal RNA, *Biochemistry 37*, 16989−16996.
8. Henn, A., Shi, S. P., Zarivach, R., Ben-Zeev, E., and Sagi, I. (2002) The RNA helicase DbpA exhibits a markedly different conformation in the ADP-bound state when compared with the ATP- or RNA-bound states, *J. Biol. Chem. 277*, 46559−46565.
9. Diges, C. M., and Uhlenbeck, O. C. (2001) *Escherichia coli* DbpA is an RNA helicase that requires hairpin 92 of 23S rRNA, *EMBO J. 20*, 5503−5512.
10. Tsu, C. A., Kossen, K., and Uhlenbeck, O. C. (2001) The *Escherichia coli* DEAD protein DbpA recognizes a small RNA hairpin in 23S rRNA, *RNA 7*, 702−709.
11. Hiratsuka, T. (1983) New ribose-modified fluorescent analogues of adenine and guanine nucleotides available as substrates for various enzymes, *Biochim. Biophys. Acta. 742*, 496−508.
12. Gill, S. C., and von Hippel, P. H. (1989) Calculation of protein extinction coefficients from amino acid sequence data, *Anal. Biochem. 182*, 319−326.
13. Pugh, G. E., Nicol, S. M., and Fuller-Pace, F. V. (1999) Interaction of the *Escherichia coli* DEAD box protein DbpA with 23 S ribosomal RNA, *J. Mol. Biol. 292*, 771−778.
14. Birdsall, B., King, R. W., Wheeler, M. R., Lewis, C. A., Jr., Goode, S. R., Dunlap, R. B., and Roberts, G. C. (1983) Correction for light absorption in fluorescence studies of protein−ligand interactions, *Anal. Biochem. 132*, 353−361.
15. Roy, S. (2004) Fluorescence quenching methods to study protein-nucleic acid interactions, *Methods Enzymol. 379*, 175−187.
16. Walker, J. E., Saraste, M., Runswick, M. J., and Gay, N. J. (1982) Distantly related sequences in the alpha- and beta-subunits of ATP synthase, myosin, kinases and other ATP-requiring enzymes and a common nucleotide binding fold, *EMBO J. 1*, 945−951.
17. Abel, R. L., Haigis, M. C., Park, C., and Raines, R. T. (2002) Fluorescence assay for the binding of ribonuclease A to the ribonuclease inhibitor protein, *Anal. Biochem. 306*, 100−107.
18. Gutfreund, H. (1995) *Kinetics for the Life Sciences: Receptors, Transmitters and Catalysts*, Cambridge University Press.
19. Talavera, M. A., and De La Cruz, E. M. (2004), unpublished experiments.
20. Henn, A., Akabayov, B., and Sagi, I. (2004), unpublished experiments.
21. Spolar, R. S., and Record, M. T., Jr. (1994) Coupling of local folding to site-specific binding of proteins to DNA, *Science 263*, 777−784.
22. Baldwin, R. L. (1986) Temperature dependence of the hydrophobic interaction in protein folding, *Proc. Natl. Acad. Sci., U.S.A. 83*, 8069−8072.
23. Bergqvist, S., Williams, M. A., O'Brien, R., and Ladbury, J. E. (2004) Heat capacity effects of water molecules and ions at a protein-DNA interface, *J. Mol. Biol. 336*, 829−842.
24. Robblee, J. P., Olivares, A. O., and De La Cruz, E. M. (2004) Mechanism of nucleotide binding to actomyosin VI − Evidence for allosteric head−head communication, *J. Biol. Chem. 279*, 38608−38617.
25. Nowak, E., and Goody, R. S. (1988) Kinetics of adenosine 5′-triphosphate and adenosine 5′-diphosphate interaction with G-actin, *Biochemistry 27*, 8613−8617.
26. Eccleston, J. F., and Trentham, D. R. (1979) Magnesium ion dependent rabbit skeletal muscle myosin guanosine and thioguanosine triphosphatase mechanism and a novel guanosine diphosphatase reaction, *Biochemistry 18*, 2896−2904.
27. Moore, K. J., and Lohman, T. M. (1994) Kinetic mechanism of adenine nucleotide binding to and hydrolysis by the *Escherichia coli* Rep monomer. 2. Application of a kinetic competition approach, *Biochemistry 33*, 14565−14578.
28. Wu, P., and Brand, L. (1994) Resonance energy transfer: methods and applications, *Anal. Biochem. 218*, 1−13.
29. Stryer, L. (1978) Fluorescence energy transfer as a spectroscopic ruler, *Annu. Rev. Biochem. 47*, 819−846.
30. Bujalowski, W., and Jezewska, M. J. (2000) Kinetic mechanism of nucleotide cofactor binding to *Escherichia coli* replicative helicase DnaB protein. stopped-flow kinetic studies using fluorescent, ribose-, and base-modified nucleotide analogues, *Biochemistry 39*, 2106−2122.
31. Jeong, Y. J., Kim, D. E., and Patel, S. S. (2004) Nucleotide binding induces conformational changes in *Escherichia coli* transcription termination factor Rho, *J. Biol. Chem. 279*, 18370−18376.
32. Moore, K. J., and Lohman, T. M. (1994) Kinetic mechanism of adenine nucleotide binding to and hydrolysis by the *Escherichia coli* Rep monomer. 1. Use of fluorescent nucleotide analogues, *Biochemistry. 33*, 14550−14564.
33. Schneider, D. A., and Gourse, R. L. (2004) Relationship between growth rate and ATP concentration in *Escherichia coli* − A bioassay for available cellular ATP, *J. Biol. Chem. 279*, 8262−8268.
34. Polach, K. J., and Uhlenbeck, O. C. (2002) Cooperative binding of ATP and RNA substrates to the DEAD/H protein DbpA, *Biochemistry 41*, 3693−3702.
35. Geeves, M. A., and Holmes, K. C. (1999) Structural mechanism of muscle contraction, *Annu. Rev. Biochem. 68*, 687−728.
36. Lohman, T. M. (1986) Kinetics of Protein-Nucleic Acid Interactions − Use of Salt Effects to Probe Mechanisms of Interaction, *CRC Crit. Rev. Biochem. 19*, 191−245.
37. De La Cruz, E. M., and Pollard, T. D. (1995) Nucleotide-free actin: stabilization by sucrose and nucleotide binding kinetics, *Biochemistry. 34*, 5452−5461.
38. Bagshaw, C. R., Eccleston, J. F., Eckstein, F., Goody, R. S., Gutfreund, H., and Trentham, D. R. (1974) The magnesium ion-dependent adenosine triphosphatase of myosin. Two-step processes of adenosine triphosphate association and adenosine diphosphate dissociation, *Biochem. J. 141*, 351−364.
39. Neumann, L., Abele, R., and Tampe, R. (2002) Thermodynamics of peptide binding to the transporter associated with antigen processing (TAP), *J. Mol. Biol. 324*, 965−973.
40. Yamada, K. (1999) Thermodynamic analyses of calcium binding to troponin C, calmodulin and parvalbumins by using microcalorimetry, *Mol. Cell. Biochem. 190*, 39−45.
41. Wieprecht, T., Beyermann, M., and Sellig, J. (1999) Binding of antibacterial magainin peptides to electrically neutral membranes: thermodynamics and structure, *Biochemisty 38*, 10377−10387.
42. Sturtevant, J. M. (1977) Heat capacity and entropy changes in processes involving proteins, *Proc. Natl. Acad. Sci., U.S.A. 74*, 2236−2240.
43. Spolar, R. S., Livingstone, J. R., and Record, M. T., Jr. (1992) Use of liquid hydrocarbon and amide transfer data to estimate contributions to thermodynamic functions of protein folding from the removal of nonpolar and polar surface from water, *Biochemistry 31*, 3947−3955.
44. Cooper, A., Johnson, C. M., Lakey, J. H., and Nöllmann, M. (2001) Heat does not come in different colours: entropy-enthalpy compensations, free energy windows, quantum confinements, pressure perturbation calorimetry, solvation and the multiple causes of heat capacity effects in biomolecular interactions, *Biophys. Chem. 93*, 215−230.
45. Delagoutte, E., and von Hippel, P. H. (2002) Helicase mechanisms and the coupling of helicases within macromolecular machines. Part I: Structures and properties of isolated helicases, *Q. Rev. Biophys. 35*, 431−478.
46. Carmel, A. B., and Matthews, B. W. (2004) Crystal structure of the BstDEAD N-terminal domain: a novel DEAD protein from *Bacillus stearothermophilus*, *RNA 10*, 66−74.
47. Tanner, N. K., Cordin, O., Banroques, J., Doere, M., and Linder, P. (2003) The Q motif: a newly identified motif in DEAD box helicases may regulate ATP binding and hydrolysis, *Mol. Cell. 11*, 127−138.
48. Carson, M., and Bugg, C. E. (1986) Algorithm for Ribbon Models of Proteins, *J. Mol. Graphics 4*, 121−122.

BI048253I